Design of a Vibrotactile Display via a Rigid Surface

Yon Visell and Jeremy R. Cooperstock
McGill University, Centre for Intelligent Machines and CIRMMT, Montreal, Canada

ABSTRACT

This paper describes the analysis, optimized redesign and evaluation of a high fidelity vibrotactile interface integrated in a rigid surface. The main application of the embodiment described here is vibrotactile display of virtual ground surface material properties for immersive environments, although the design principles are general. The device consists of a light, composite plate mounted on an elastic suspension, with integrated force sensors. It is actuated by a single voice coil motor. The structural dynamics of the device were optimized, within constraints imposed by the requirements of user interaction, and corrected via digital inverse filtering, in order to enable accurate simulation of virtual ground materials. Measurements of the resulting display demonstrate that it is capable of accurately reproducing forces of more than 40 N across a usable frequency band from 50 Hz to 750 Hz.

Keywords: Vibrotactile display design, Vibrotactile rendering, Foot interfaces

1 INTRODUCTION

Vibrotactile display devices consist of palpable interfaces that are capable of vibrating at frequencies salient to human tactile perception, but are not necessarily capable of static force display [35]. Advantages of such displays include their low cost, power efficiency, and capability of rendering transient or textural effects accurately, at high temporal resolution, when suitable actuators are used.

1.1 Vibrotactile augmentation of floor surfaces

The work presented here concerns the design of a vibrotactile display device integrated in a rigid panel. The specific embodiment involved is an augmented floor panel designed to enable vibrotactile interaction with ground surfaces. Potential applications of such a device include the simulation of ground textures for virtual and augmented reality simulation [39] or telepresence (e.g., for remote planetary simulation), the rendering of abstract effects or other ecological cues for rehabilitation, or the presentation of tactile feedback to accompany the operation of virtual foot controls, control surfaces, or other interfaces [40]. This device constitutes a redesign and optimization of an interface that was introduced in earlier work by the authors [36]. The goal was to systematically improve its fidelity. One motivation for doing so is to avoid artifacts that can affect realism and prevent careful control of stimuli in experiments involving human vibrotactile perception. The main artifacts alleviated by the redesign are due to selective variations in the device frequency response within the range of human vibrotactile sensitivity. We have also attempted to provide enough documentation that the device, or others like it, may be produced by researchers or practitioners interested in vibrotactile display via rigid surfaces. The sections that follow present the device concept, its mechanical and electronic structure, the optimizations that were undertaken to improve its dynamic response, and an analysis of the results.

1.2 Background

The fidelity of a haptic device depends on the selection and arrangement of electronic components, and on its structural design, as has long been emphasized in the research literature on force-feedback displays. Many of the analogous questions for the design of vibrotactile (VT) displays have received less attention. The vibrotactile augmentation of touch surfaces has been widely investigated for HCI applications [24, 11, 23], although design issues affecting their perceptual transparency have often been neglected. A few examples demonstrating optimized vibrotactile device engineering [41] or software compensation of their dynamics [18] do, nonetheless, exist. Issues related to sensor and actuator selection are covered in recent reviews of haptic hardware prototyping [13], while the extensive literature on acoustic and vibration engineering provide the knowledge needed for structural dynamics optimization [22, 7, 10].

We are not aware of any prior work on the systematic design of vibrotactile floor panels for haptic interaction. Passive floor-based vibrotactile actuation has been used to present low frequency information in audiovisual display applications, for special effects (e.g., vehicle rumble), in immersive cinema or VR settings [33]. The fidelity requirements that must be met by an *interactive* haptic display are, all things being otherwise equal, higher, since its users are able to actively sample its response to actions of the feet.

Many designs for vibrotactile-augmented shoes or insoles have been proposed [19, 27, 25], but nearly all have been designed for symbolic information display (e.g., directional indicators or encoded messages) or biofeedback stimuli, rather than for presenting virtual ecological stimuli. State of the art haptic force feedback interfaces for walking [14] are capable of preserving kinesthetic degrees of freedom but are restricted to a small fraction of the bandwidth that our device achieves. As noted below, a wide bandwidth interface is advantageous for reproducing the rich variety of high-frequency force information that is generated during walking in natural environments [28].

2 DISPLAY CONCEPT AND MOTIVATION

The interface of the device (Fig. 5) consists of a rigid plate that supplies vibrations in response to forces supplied by a user's foot, via the shoe. The total normal force $F(t)$ applied to the plate by a user is measured. It can be assumed to consist of two components: isolated transients with high frequency content, generated by foot impacts with the plate, and low-frequency forces generated by active human motions, limited in bandwidth to no more than 10 Hz [3, 37]. Vibrotactile feedback is assumed to be constrained, due to actuator limitations, to frequencies greater than a minimum value on the order of 20 Hz.

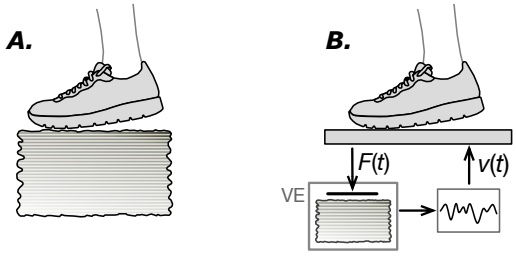

Figure 1: (*A.*) The experience of stepping onto a deformable object or surface is (*B.*) simulated via a rigid vibrotactile interface.

A haptic simulation (Fig. 1) provides feedback approximating the vibration response felt during interaction with a virtual object. Our rendering algorithms are of admittance type, computing velocities of displacement in response to forces applied to the virtual

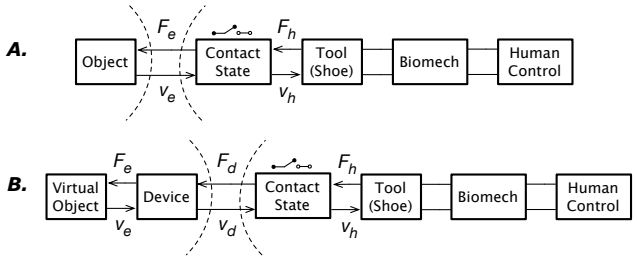

Figure 2: The haptic display concept. (*A.*) A real system being simulated involves interaction with an object via a tool (the shoe) in a user's grasp. The user exerts a force $F_h(t)$ and experiences a vibration $v_h(t)$. (*B.*) The display mediates interaction with the virtual environment. The dashed lines demarcate system components associated with the object, or its haptic presentation, from those of the user.

object. An example of such an algorithm is described in Sec. 2.2. As with most vibrotactile displays, vibrations are presented in open loop fashion. During the course of interaction, user coupling to the device interface is expected to vary from no contact to full-foot contact with large forces. In the virtual environment, interaction is mediated by an idealized proxy that is constrained to a constant region on the virtual object surface, at which force is applied. In these respects, the contact state is entirely modeled in the real world (Fig. 2). In other words, user-supplied forces (zero or otherwise), as measured by the device, are continuously mapped to the simulation, and there is no modeling of contact variation within the virtual environment.

2.1 Transparency

In order to ensure perceptual transparency of the display, the admittance of the virtual object it presents should resemble as closely as possible that of its real counterpart. As illustrated in Figure 2, this requires that the (velocity) feedback generated from forces applied to the virtual object closely match those produced by interaction with the real one, and that the device transfer function $H_d(s)$ be as close to unity as possible. Here, we refer to the free (unloaded) response of the display, corresponding to components to the left of the dashed lines in Fig. 2. When coupled to a user, the acceleration response of the interface will be modified due to the state of contact between the user and plate, and the biomechanical dynamics of the user (measurements are presented in Sec. 5). These variations are beneficial in allowing our device to mimic natural variations in the response of a real object that is being simulated. The dependence of the virtual object response on the force exerted by the user is incorporated explicitly, because our haptic rendering models are force driven. This contrasts with the case of impedance based displays, where only position (or velocity) is measured. In order to ensure transparent open-loop playback of haptic events in settings like the latter, the device's response requires grip-dependent corrections that account for changes in the display admittance due to grip or arm dynamics [9]. Further discussion is provided in Sec. 4.5.

2.2 Application to normal force texture simulation

An example application motivating the design reported here is the display of normal force textures, in the form of high frequency vibrations simulating the feel of stepping onto natural ground materials [36]. When a shoe steps onto porous materials like soil or snow, it is subjected to interactions that can include: viscoelastic components, describing the recoverable deformation of the volume of the ground surrounding the contact interface; transient shock components, from the impact of toe and heel against the ground; and plastic components from the collapse of air pockets, brittle structures or granular force chains, resulting in unrecoverable deformation [6, 29]. Combinations of such effects give rise to low-frequency forces and high frequency, texture-like vibrations that are characteristic of human walking on different surfaces [28]. Figure 3 presents an example of force and vibration data acquired from one footstep on a gravel surface. Because the vibration signature is continuously coupled to the force input over time in such examples, there is no straightforward way to convincingly use recorded footstep vibrations for vibrotactile rendering, although more flexible granular sound-synthesis methods could be used [1, 5]. For the modeling of simpler interactions, involving impulsive contact with solid materials, recorded transient playback techniques could be used [18].

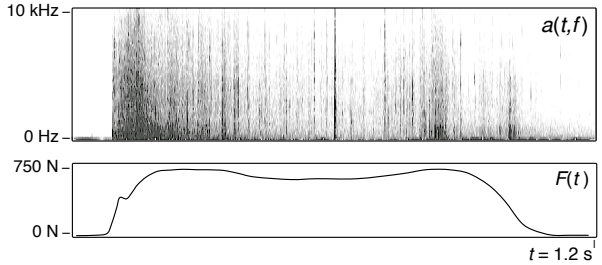

Figure 3: Vibration spectrogram $a(t,f)$ and normal force $F(t)$ measured from one footstep onto rock gravel (Authors' recording). Note the discrete, broadband impact events evidenced by vertical lines in the spectrogram.

We briefly summarize one approach we have taken to the haptic synthesis of interaction with such surfaces. It is based on fracture mechanics, which has also proved useful for modeling other types of haptic interaction involving damage [12, 20]. Figure 4 illustrates the continuum model and a simple mechanical analog used for synthesis. In the stuck state, the surface has stiffness $K = k_1 + k_2$ and is governed by:

$$F(t) = m\ddot{x} + b\dot{x} + K(x - x_0), \quad x_0 = k_2\xi(t)/K \tag{1}$$

where $\xi(t)$ represents the net plastic displacement up to time t. A Mohr-Coulomb yield criterion is applied to determine slip onset: When the force on the plastic unit exceeds a threshold value (which may be constant or noise-dependent), a slip event generates an incremental displacement $\Delta\xi(t)$, along with an energy loss of ΔW representing the inelastic work of fracture growth. Slip displacements are rendered as discrete transients, using an event-based approach [18]. High frequency components of such transient events are known to depend in detail on the materials and forces of interaction, and we model some of these dependencies when synthesizing the transients [38].

A high fidelity vibrotactile display such as that presented here is useful for reproducing such phenomena without artifacts.

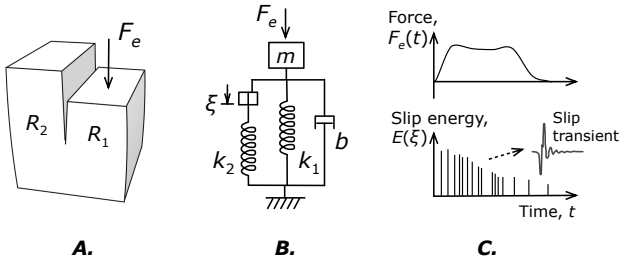

Figure 4: Normal force texture synthesis. *A.* A fracture mechanics approach is adopted. A visco-elasto-plastic body undergoes shear sliding fracture due to applied force F_e. *B.* A simple mechanical analog for the generation of slip events $\xi(t)$ in response to F_e. *C.* For vibrotactile display, each slip event is rendered as an impulsive transient using an event-based approach.

3 COMPONENTS

3.1 Mechanical Structure

The mechanical design is broadly similar to that of the original device, but accounts better for both the static and dynamic performance requirements for the display. The top plate provides an interface to the body, which in the case of our device is assumed to consist of a foot wearing a shoe. Statically, the device must resist bending when loaded vertically by a force of several hundred Newtons. The rigid deflection of the plate under this load must be minimized subject to the constraint that the plate be able to vibrate freely. This trade-off is analyzed in Section 4.3.

The top plate consists of a commercially manufactured aluminum honeycomb sandwich panel component (Museum Services Corp model 0513 SSP) with dimensions $30.4 \times 30.4 \times 2.54$ cm and a weight of 400 g. The panel has aluminum facings with a thickness of 0.08 cm. This material was selected for its high bending stiffness to weight ratio. The panel sides are closed with a basswood frame to eliminate acoustic emissions or deformations that otherwise result from small deflections of the honeycomb at the edges of the panel. The plate is supported by cylindrical SBR rubber elastic elements positioned as shown in Fig. 5. In dynamic or multi-tile configurations, a retaining socket surrounding the elastic support (not present in the figure) is used to keep the plate from changing position. The actuator is mounted via an aluminum bracket bonded to the center underside of the plate.

3.2 Sensing

In order to render an interactive response from a virtual ground surface using the kinds of models we have developed (Sec. 2.2), it is necessary to capture the normal force applied to the tile by the user's foot. Positioning the force sensors beneath the plate is feasible, since the bandwidth of the force applied to the plate by the user is limited. In the design presented here, the sensors are furthermore positioned beneath the elastic suspension of the device, so as to better isolate them from the actuators.

Force sensing is performed via four load cell force transducers (Measurement Systems model FX19) located below the vibration mount located under each corner of the plate. Although the cost for outfitting a single-plate device with these sensors is not prohibitive, many of the applications we have in mind consist of two dimensional $m \times n$ arrays of tiles, requiring a number $N = 4mn$ of sensors. As a result, in a second configuration, four low-cost resistive force sensors (Interlink model 402 FSR) are used in place of load cells. After conditioning, the response of these sensors to an applied force is nonlinear, and varies up to 25% from part to part (according to manufacturer ratings). Consequently, a measurement and subsequent linearization and force calibration of each is performed, using a calibrated load cell force sensor (details are provided in a separate publication [39]). After such a calibration, a linear response accurate to within 5% can be obtained using low cost parts.

3.3 Actuation

The tile is actuated by a single Lorentz force type inertial motor (Clark Synthesis model TST429) with a nominal impedance of 6 Ohms. The actuator is coupled to the tile by a 1.25 cm diameter threaded rod interfacing with an aluminum bracket, as shown in Fig. 5. The actuator has a usable bandwidth of about 25 Hz to 20 kHz, and is capable of driving the plate above strongly enough to quickly produce numbness in the region of the foot that is in contact with the tile.

3.4 Electronics

Analog data from the force sensors is conditioned, amplified, and digitized via a custom acquisition board, based on an Altera FPGA, with 16-bit analog-to-digital converters. Data from each sensor is sampled at a rate of 1 kHz and transported to a host computer over UDP via the board's 10 Mbps Ethernet interface. Digital to analog conversion of the signal driving the actuator is performed using a low noise 24-bit, 96 kHz audio interface (Edirol model FA-101), and amplification is performed using a compact, class-D audio amplifier based on the Tripath TK2050. The amplifier is rated as capable of providing 100 W to a nominal 4 Ohm actuator impedance.

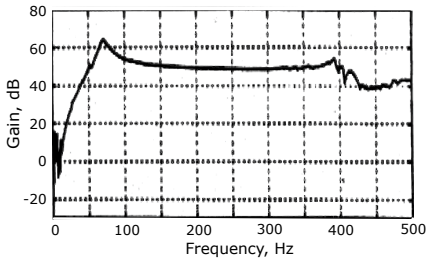

Figure 6: Typical acceleration frequency response of the Clark Synthesis TST family of actuators (manufacturer supplied data, reproduced with permission).

4 DYNAMIC RESPONSE

The main factors affecting the dynamic response of the device are the actuator characteristics, the dynamics of the rigid plate, and that of the elastic suspension. In a suitable regime, one may regard these as lumped linear systems, with respective Laplace transform domain transfer functions $H_a(s), H_p(s)$ and $H_s(s)$. The corresponding model device transfer function can be given by $H_d(s) = H_a(s)H_p(s)H_s(s)$. However, the spatial configuration of these elements relative to each other also contributes to the structural dynamics of the display.

4.1 Actuator Response

Fig. 6 shows a typical amplitude frequency response for this family of actuators. The data was acquired from an accelerometer attached to the mounting bold, with the actuator attached to a rigid wooden surface. The shape of this nominal response affects that of our device (Sec. 5).

4.2 Plate Response

The contribution of the interface plate to the dynamic response of the device can be predicted in terms of the vibrational characteristics of the plate, and the coupling between plate and actuator.

4.2.1 Free response

In the case of a homogeneous, isotropic plate, the free vibrations of interest are governed by a partial differential equation for bending wave displacements. In the thin plate approximation, it is [10]:

$$\rho h \frac{\partial^2 z}{\partial t^2} + D\nabla^4 z = 0, \quad D = \frac{Eh^3}{12(1-\nu^2)} \tag{2}$$

Here, $z = z(\mathbf{r}, t)$ is displacement, $\mathbf{r} = (x, y)$ is a position on the tile surface, t is time, E and ν are the Young's modulus and Poisson's ratio of the plate material, ρ is its mass density, and h is the plate thickness, D is known as the flexural stiffness, and we neglect effects of damping.

Below the first resonant frequency of the plate, f_1, the vibrational response is well approximated by that of an ideal, rigid mass coupled to an elastic suspension (Sec. 4.3 below). Since we seek a usable display bandwidth with an upper limit of 1 kHz, we want to ensure that $f_1 > 1$ kHz. For a rectangular, homogeneous, isotropic plate, the frequencies of the normal modes of bending oscillation

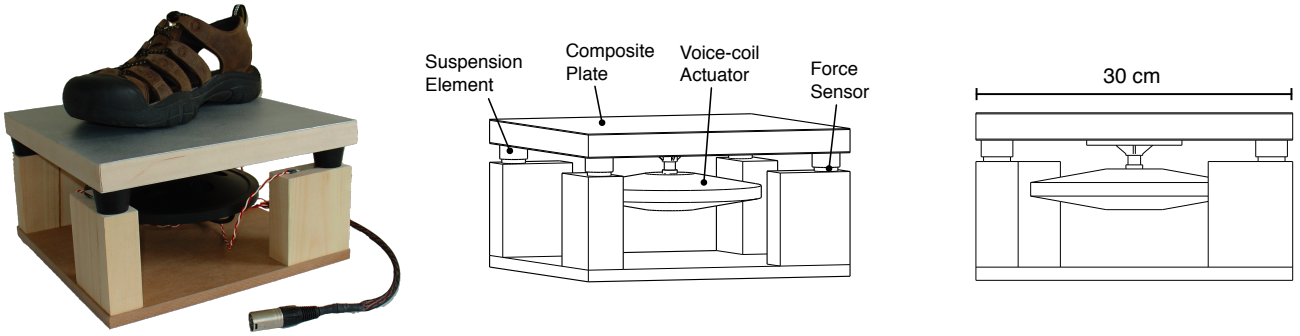

Figure 5: Vibrotactile floor interface hardware for a single tile unit. Left: Photo with large mens' shoe, showing representative size. The model shown is based on the low-cost force sensing resistor option. The cable in the foreground interfaces the sensors with the data acquisition unit. Middle: View showing main components. Right: Side view with top dimension.

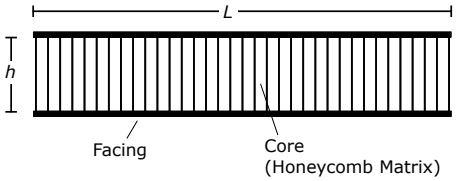

Figure 7: A composite sandwich plate, shown in profile (side view). It consists of a stiff, solid facing material bonded (typically laminated) to a lightweight core, such as a metal or kevlar honeycomb matrix.

are of the form [10]:

$$f(k) = \frac{hk^2}{2\pi}\sqrt{\frac{D}{\rho h}}, \quad k \propto L^{-1} \tag{3}$$

Here, k is the magnitude of the wavenumber vector $\mathbf{k} = (k_x, k_y)$ of the oscillation, and L^{-1} is the inverse length of the plate, and x and y are the directions tangent to the plate surface parallel to its edges. For pure simply supported boundary conditions (which are never achieved in practice), $k_x = m\pi/L$ and $k_y = n\pi/L$, where m and n are positive (non-zero) integers [10]. The lowest frequency mode is $f_1 = f(|\mathbf{k}_1|)$, with $\mathbf{k}_1 = (\pi/L, \pi/L)$. The amplitudes of the normal modes are

$$\eta_{mn}(\mathbf{r}) = \sin(k_x x)\sin(k_y y) \tag{4}$$

After inserting the form of D from Eq. 2 into Eq. 3, Poisson's ratio ν contributes a factor $(1-\nu^2)^{-1/2}$ to $f(k)$. This factor lies in a range from 1.0 to 1.16 for solid materials such as are considered here, so in a first approximation we may ignore it. In order to maximize the frequency $f(k)$ for any given value of the wavenumber magnitude k, and given plate geometric properties L and h, the plate material should be selected to possess a large Young's modulus E and low mass density ρ. Solid, isotropic materials such as metals can achieve a high stiffness, but their mass density is typically commensurately higher, which is a limitation. In addition, their mass grows linearly with thickness, making them less efficient to actuate. In practice, for a solid plywood plate (light enough to be efficiently actuated) with dimensions 30.4 cm × 30.4 cm × 3.75 cm, one finds $f_1 \approx 400$ Hz, which falls short of the design target.

4.2.2 Composite plate

A class of structures that achieves higher stiffness-to-mass ratios than is possible with uniform solids is that of composite sandwiches. Such a panel is formed via the use of thin layers of stiff solid material bonded to a lightweight core. Fig. 7 illustrates a composite sandwich of the type used in our device. The core consists of an aluminum honeycomb matrix, while the facing materials consist of aluminum sheet. The bending stiffness of such a material is approximately given by $E \approx \sqrt{3}E_f t_f/h$ [15], where E_f is the Young's modulus of the facing material, t_f is the thickness of the facing material, and h is the core thickness (Fig. 7). To a first approximation, the frequencies of the normal modes of bending oscillation of such a composite sandwich plate can be obtained[1] substituting this expression for E into Eq. 3. The resulting frequencies are:

$$f(k) = \frac{k^2}{2\pi}\sqrt{\frac{E_f t_f h}{12\rho}}, \quad k \propto L^{-1} \tag{5}$$

Again, the admissible values of k depend on the boundary conditions. This equation (which is valid only for thin facings $t_f \ll h$) depends on the stiffness E_f of the facing material and the average mass density of the entire panel. For our device, assuming idealized boundary conditions, the minimum value of k is $\pi\sqrt{2}/L$ (see Sec. 4.4). The other factors are given by: $h = 2.5$ cm, $t_f = 0.083$ cm, $E_f \approx 60$ GPa, and $\rho \approx 170$ kg / m^3. For these values, Eq. (5) yields $f_1 \approx 845$ Hz. This overestimates the measured value of f_1 for our device by approximately 10% (Sec. 5).

4.2.3 Actuator coupling

The actuated plate is driven by a surface force (pressure) distribution $F(\mathbf{r},t)$, and the resulting governing equation possesses a driving term:

$$\rho h\frac{\partial^2 z}{\partial t^2} + D\nabla^4 z = F(\mathbf{r},t) \tag{6}$$

For our device, the latter can be modeled as a $F(\mathbf{r},t) = F(t)\phi(\mathbf{r})$, where $F(t)$ is the actuator force amplitude, and $\phi(\mathbf{r})$ approximates a spatial Dirac delta function $\delta(\mathbf{r}-\mathbf{r}_0)$ centered at the tile midpoint. Generalizing slightly, one can consider the case of N independent point actuators at locations $\mathbf{r}_i$, in which case $F(\mathbf{r}) = \sum_{i=1}^{N} F_i(t)\delta(\mathbf{r}-\mathbf{r}_i)$, where F_i is the force signal from the ith actuator.

An arbitrary displacement $z(\mathbf{r},t)$ can be expanded in the normal modes $\eta_{mn}(\mathbf{r})$ of vibration, yielding modal coordinates $Z_{mn}(t)$ defined by:

$$z(\mathbf{r},t) = \sum_{m,n\geq 0} Z_{mn}(t)\eta_{mn}(\mathbf{r}), \quad \text{where} \tag{7}$$

$$Z_{mn}(t) = \int z(\mathbf{r},t)\eta_{mn}(\mathbf{r})d^2\mathbf{r} \tag{8}$$

[1] The authors did not find this expression for $f(k)$ in the research literature, but approximations like it are presumably well-known.

In these coordinates, the physical equation is [22]:

$$\left(\frac{\partial^2}{\partial t^2}+\omega_{mn}^2\right)Z_{mn}(t)=\sum_i \eta_{mn}(\mathbf{r}_i)F_i(t) \tag{9}$$

where ω_{mn} is the angular frequency of mode (m,n). Modes having nodes at the actuator location, $\eta_{mn}(\mathbf{r}_i)=0$, satisfy the homogeneous form of Eq. (9), so are not excited by the corresponding actuator signal, and instead contribute antiresonances to the device response. As shown in Sec. 5, the bandwidth of our device is essentially limited by the antiresonance near 775 Hz for $(m,n)=(1,1)$.

4.3 Elastic Suspension

The actuator is designed to supply a force only along the direction in which it is attached, so we are primarily interested in normal modes of oscillation in the z-direction. To a first approximation, the elastic (SBR rubber) suspension may be treated as a linear, lumped element with stiffness K in the z-direction, coupled to a rigid plate with total mass M (Fig. 8). For small displacements, this stiffness is given by $K=EA/h$, where E is the Young's modulus of the suspension element, A is its vertical surface area, and h is its height. When the plate is not subjected to load from a foot, the mass $M=M_0$ is due to the plate and actuator. For the device described here, $M_0=2.7$ kg.

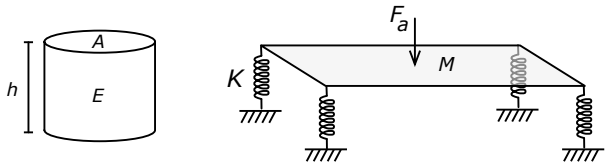

Figure 8: Left: Geometry of one elastic suspension element with height h, cross-sectional area A, and elastic modulus E. Right: Lumped model of the tile-suspension system. F_a is the actuator supplied force, $K=EA/h$ is the stiffness of a suspension element, and M is the combined mass of the actuator and tile.

Due to the symmetric placement of the actuator, there is a single dominant normal mode of oscillation, in which all suspension elements are driven in-phase in the vertical direction. The resonant frequency of this mode in the unloaded condition is given by $f_0=(2\pi)^{-1}\sqrt{4K/M_0}=(2\pi)^{-1}\sqrt{4EA/(hM_0)}$. Above this frequency, the gain of the transfer function factor due to the suspension, $H_{susp}(f)$, is expected to be approximately constant.

A softer suspension leads to a larger response bandwidth (i.e., one with a lower frequency extent) but also to a higher static deflection δz under a load F from a foot. The latter two are related by $\delta z=F/K=Fh/(EA)$. As nominal design specifications, we aimed to select E,A and h so that $f_0\le 50$ Hz, so that the passband would overlap most of the frequency range of sensitivity of the FA II (Pacinian) tactile mechanoreceptors in the foot. The latter closely resembles the range for those in the hand [16, 34]. In addition, we aimed to achieve a worst-case static deflection $\delta z\le 5$ mm under a load of $F=1000$ N, corresponding to a large human balanced at one corner. Both f_0 and δz depend only on the ratio A/h. For convenience, we choose the cross sectional area A of the suspension element to match that of the force sensor. To choose the remaining parameters, we perform a simultaneous grid search on h and E to minimize f_0 and δz. Figure 9 illustrates the dependence of f_0 and δz on E for a representative set of selected parameter values, i.e., $A=8$ cm^2 and $h=2.5$ cm. We selected SBR rubber vibration mounts with geometry and Young's modulus $E=2.0$ MPa consistent with this optimization. As shown in the figure, the resulting system is expected to achieve $f_0\approx 49$ Hz and $\delta z\approx 4.5$ mm.

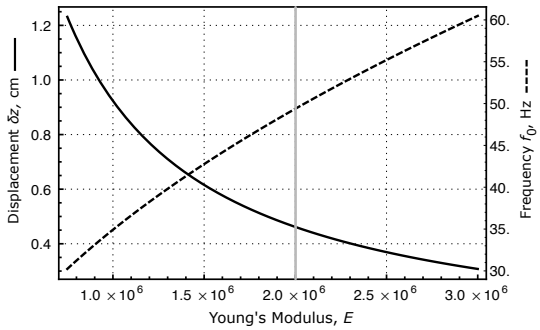

Figure 9: Resonant supension frequency f_0 and static deflection δz vs. Young's modulus for the system model with $A=8$ cm^2 and $h=2.5$ cm. The value $E=2$ MPa (grey vertical line) satisfies $f_0<50$ Hz and $\delta z<5$ mm.

4.4 Simulation

The vibrational characteristics of the tile-actuator system were simulated using finite element method (FEM) analysis. A three-dimensional geometric model of the device was designed, incorporating the sandwich panel, actuator (modeled as a homogeneous cylindrical mass), actuator bracket and connecting rod, elastic elements, and supporting structure. Material properties were assigned approximating those of the device itself, with the core honeycomb matrix replaced by a homogeneous solid with an equivalent density. Although this model entails a number of approximations, the qualitative results were expected to be correct.

4.4.1 Eigenfrequency analysis

At high frequencies, the resonant modes of the plate itself are observed. The first two are shown in Fig. 10. The lowest frequency mode has wavenumber $\mathbf{k}=(1,1)$, while the next highest resonance shown appears to correspond to a plate-induced mixture of the $(0,2)$ and $(2,0)$ modes. Their frequencies, 896 Hz and 1032 Hz, lie at a ratio of about 1.15:1.

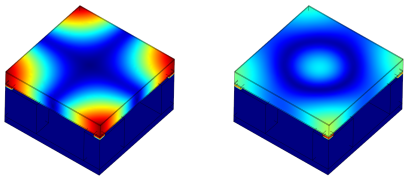

Figure 10: Visualization of the first two resonant modes of the device due to the bending mode vibrations of the plate as identified in the FEM analysis. The ring mode (right side) arises from the mixing of the plate modes indexed by the integers shown [10]. The frequencies are 896 Hz and 1032 Hz.

At low frequencies, a series of six resonances at frequencies of 28, 45, 51, and 77 Hz is observed, corresponding to deformations of the elastic support elements, in agreement with the lumped model of Sec. 4.3. The number of resonances exactly matches the six degrees of freedom of perturbation of the rigid tile. The deformation shapes recovered from the FEM analysis show that the 45 Hz resonance corresponds to oscillation in the direction normal to the plate surface; it is expected to dominate when the display is driven by the actuator.

4.4.2 Frequency response simulation

The FEM simulation of the frequency response was performed with a sinusoidal driving signal originating at the actuator. The z-axis

acceleration was measured at several points on the surface of the plate, with the results shown in Fig. 11. As determined above, the cross-shaped mode gives rise to an antiresonance, due to the actuator location. The magnitude effect of these resonances, and to a secondary degree their frequency, depends substantially on the measuring point.

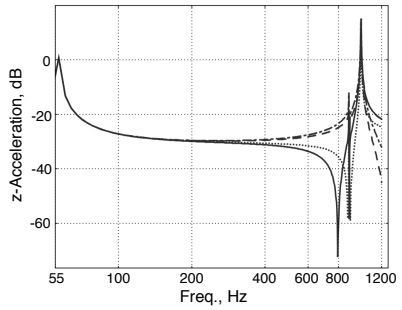

Figure 11: Result of a FEM analysis of the acceleration response of the device as measured at four different points on the plate surface. At frequencies below the first resonant mode, the device response is approximately constant over the surface of the plate.

4.5 Modeling user-supplied loads

We have so far discussed the response of the device without accounting for effect of to its user. According to the haptic interaction model adopted here (Sec. 2) it is correct to ignore the influence of this load, as transparency requires that the free (unloaded) display transfer function approach unity. However, in other circumstances it may be desirable to compensate for variations in the display response due to user contact. Examples where this might be the case include passive vibrotactile stimulation for tactile communication or psychophysical experiments, or for use with impedance-based rendering algorithms or simulations that explicitly model user contact conditions in the virtual environment. At the frequencies of

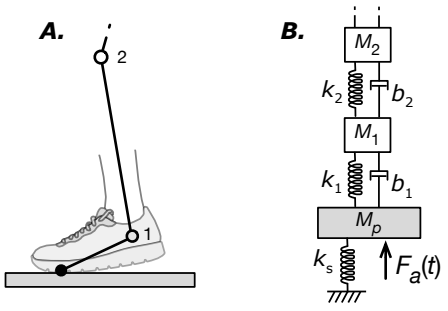

Figure 12: (*A.*) A simplified model of a user-supplied load can be provided in the form of a link-segment model or (*B.*) its equivalent mechanical network, coupled to the display device. $F_a(t)$ is force applied by the actuator.

interest, a user may be modeled as a passive viscoelastic mechanical system. Figure 12 shows a simple link-segment biomechanical model and equivalent mechanical network coupled to the display. Physiologically, biomechanical properties such as leg joint stiffness cannot be regarded as static or linear during movement, as muscular activation regularly modulates the dynamic properties of the lower limbs during activities on foot [26, 21, 8]. However, as a typical leg stiffness value one may take $k = 10$ kN/m [26]. Upon adopting a simple, single mass-spring-damper model with this value, and assuming an effective mass of 50 kg, one finds that a user-supplied load should suppress frequencies in the vicinity of 200-250 Hz. This prediction is consistent with the load-dependent frequency response measurements we report below (Sec. 5.1). Similar grip-dependent effects are observed to affect manually operated haptic [17, 9] and vibrotactile [41] devices.

5 Evaluation

As noted in Sec. 2.1, our assessment of the transparency of this device is based on the extent to which the unloaded transfer function of the display approximates unity over the range of perceptually salient frequencies. We focus here on the flatness of the magnitude frequency response. The vibrotactile sense is sensitive to phase differences [2], and it is possible that a vibrotactile display may contribute enough phase distortion to affect perception, particularly where transient signal components are concerned. However knowledge about vibrotactile sensitivity to temporal phase distortion is incomplete, and, as far as we are aware, phase linearity has never been used to evaluate vibrotactile displays. It is nonetheless an important consideration in the related field of loudspeaker design.

5.1 Frequency response measurement

The magnitude frequency response of the device was measured by driving the plate with the actuator using the chirp method, with a slow sinusoidal frequency sweep (rate of 100 Hz / s). Measurement was performed using a piezoelectric accelerometer (AKG model CP-411) bonded to the top surface of the plate, as described in the caption of Fig. 13. Frequency response measurements were taken for several different foot-plate contact conditions, while the foot was wearing a rubber soled shoe. As noted above, these contact conditions modify the impedance of the display, altering its response. The results are shown in Fig. 13.

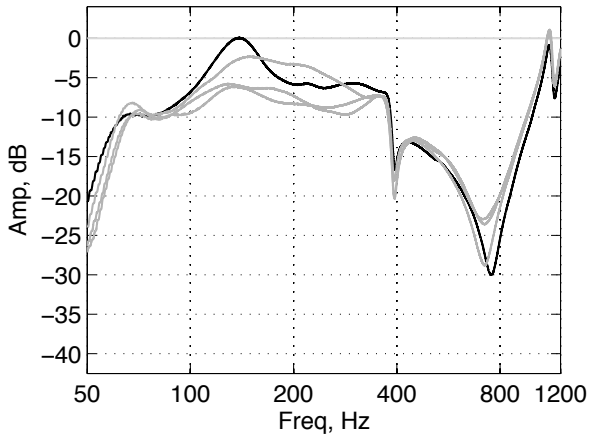

Figure 13: The measured log magnitude frequency response of the display. Measurements were taken at a point equidistant from the plate center and edge, on a line through the center, 15 degrees from the diagonal. The free response is shown with a black line, and other foot-floor contact conditions with varying load applied via the foot are shown in gray.

The variation in the magnitude frequency response below 80 Hz is, following the analysis above, likely to be attributed to a combination of the resonant modes of the vibration suspension and the actuator response (Fig. 6). The antiresonance around 775 Hz and the resonance near 1100 Hz are due to the two lowest frequency normal modes of the plate (Fig. 10) identified above. Variation in the range from 70 Hz to 700 Hz can be attributed in part to the actuator response. The latter (Fig. 6) includes a resonance near 70 Hz and additional coloration above 380 Hz, likely accounting for the smaller notch seen in the measurements. Through additional measurements with a calibrated accelerometer (Analog devices model

ADXL 320), it was determined that a force of 40 N could be transmitted at all frequencies between 50 and 750 Hz. Another pertinent quantity, nonlinear distortion, was estimated from measurements at 300 Hz to be slightly more than 5% (mean absolute percent error) up to a force of 30 N.

5.2 Digital correction

It is possible to improve the nominal frequency response $H_d(f)$ of the display by filtering the actuator signal $F(t)$ via a suitably designed linear, time-invariant corrective filter, H_c. Here, we concentrate on the magnitude only: H_c is designed so that the corrected device frequency response $H_{d'}(f) = H_d(f)H_c(f) \approx g$ in the band of interest, where g is a constant gain factor.

Since such a filter lacks any spatial dependency, correction is most effective below the first resonant frequency of the device, f_1, because above it the device transfer function varies across the surface of the plate (Fig. 11). As a result, correction is primarily useful for compensating factors, such as actuator characteristics, that can be treated as lumped parameter system elements.

We designed the inverse filter H_c to equalize the device response in the frequency range from $f = 50$ Hz to 750 Hz. It was implemented digitally as an IIR filter of order N, which was estimated using the least p-th norm optimization method [32]. Figure 14 shows a comparison of the original (free) frequency response of the device with responses corrected by filters of order $N = 10$ and 14. In the latter case, the response is flat in a passband with -10 dB roll off near 50 Hz and 750 Hz.

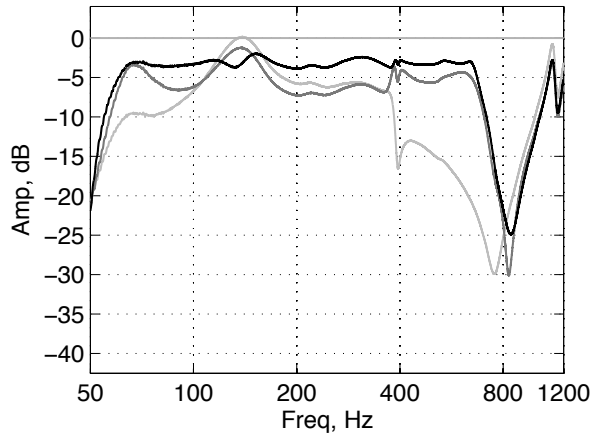

Figure 14: Measured device response without foot contact, uncorrected (lightest gray) and with correction by digital IIR filters of order $N = 10$ (medium gray) and $N = 14$ (black).

6 Conclusion

We have presented a vibrotactile display device integrated in a rigid surface, consisting of an actuated and instrumented floor tile. The analysis considered factors affecting the bandwidth of the device, including the response of the elastic suspension and rigid plate, the actuator coupling, and the static deflection of the suspension under load by a human foot. The plate was implemented as a lightweight composite sandwich panel constructed from aluminum honeycomb. A digital filter was designed to compensate for artifacts in the measured frequency response. The device allows for accurate reproduction of frequencies between about 50 and 750 Hz.

The device is simple, and designed to be easily reproducible or adaptable to the demands of various applications or research tasks [37, 38]. Formulae such as Eq. (5) indicate how the response characteristics of the display can be expected to scale with system dimensions.

Despite these results, a number of areas can be identified in which the device might be improved. They include:

- *Plate material selection:* As presented in the analysis above, a composite panel similar to that used here, but constructed from a honeycomb core with larger core thickness h, and facing thickness t_f would achieve a usable bandwidth that extends to higher frequencies. The first resonant frequency of the plate scales as $\sqrt{t_f h}$ in the thin plate approximation (which will require corrections if the plate or facings are too thick).

- *Actuator design:* The large voice coil actuator used in the present device introduces significant coloration in the frequency response of the device, much of which can be equalized. A better response may be achieved through the use of smaller, more efficient voice coil motors coupled to the structure in a spatial configuration chosen to optimize the device transfer function.

- *Vibration control:* Active structural vibration control strategies exist that could improve the fidelity of such a display using arrays of surface mounted sensors and actuators, together with closed-loop controllers [4, 30, 31]. Such techniques might be used to achieve accurately controlled vibrational responses under a wider array of contact loads.

In ongoing research in our lab, the device is being utilized to study the rendering and display of virtual ground surface properties, related aspects of haptic perception, and the integration of such display components in multimodal virtual and augmented reality environments [39].

Acknowledgements

We thank Vincent Hayward and Guillaume Millet for useful discussions, and the anonymous reviewers for their helpful comments. The authors gratefully acknowledge support from the MDEIE of Quebec for the EU FP7 project NIW (no. 222107). The first author acknowledges support from the ESF COST Action on Sonic Interaction Design (no. IC0601).

References

[1] S. Barrass and M. Adcock. Interactive granular synthesis of haptic contact sounds. In *AES 22nd International Conference on Virtual, Synthetic and Entertainment Audio*, 2002.

[2] S. Bensmaia and M. Hollins. Complex tactile waveform discrimination. *The Journal of the Acoustical Society of America*, 108:1236, 2000.

[3] G. Burdea and M. Akay. *Force and touch feedback for virtual reality*. Wiley New York, 1996.

[4] K. Chandrashekhara and A. Agarwal. Active vibration control of laminated composite plates using piezoelectric devices: a finite element approach. *Journal of Intelligent Material Systems and Structures*, 4(4):496, 1993.

[5] A. Crossan, J. Williamson, and R. Murray-Smith. Haptic granular synthesis: Targeting, visualisation and texturing. In *Proc. Intl Symposium on Non-visual & Multimodal Visualization*, pages 527–532, 2004.

[6] S. Dixon and A. Cooke. Shoe-Surface Interaction in Tennis. *Biomedical engineering principles in sports*, page 125, 2004.

[7] F. Fahy. *Foundations of engineering acoustics*. Academic Press, 2001.

[8] C. Farley and O. Gonzalez. Leg stiffness and stride frequency in human running. *Journal of Biomechanics*, 29(2):181–186, 1996.

[9] J. Fiene, K. Kuchenbecker, and G. Niemeyer. Event-based haptics with grip force compensation. In *Proc IEEE Haptic Symposium*, 2006.

[10] N. Fletcher and T. Rossing. *The physics of musical instruments*. Springer Verlag, 1998.

[11] M. Fukumoto and T. Sugimura. Active click: tactile feedback for touch panels. In *CHI'01 extended abstracts*, pages 121–122. ACM, 2001.

[12] V. Hayward. Physically-based haptic synthesis. In M. Lin and M. Otaduy, editors, *Haptic Rendering: Foundations, Algorithms and Applications*. AK Peters, Ltd, 2007.

[13] V. Hayward and K. Maclean. Do It Yourself Haptics: Part I. *IEEE Robotics & Automation Magazine*, page 89, 2007.

[14] J. Hollerbach. Locomotion interfaces and rendering. *Haptic Rendering: Foundations, Algorithms and Applications. AK Peters, Ltd*, 2008.

[15] J. Kee Paik, A. Thayamballi, and G. Sung Kim. The strength characteristics of aluminum honeycomb sandwich panels. *Thin-walled structures*, 35(3):205–231, 1999.

[16] P. M. Kennedy and J. T. Inglis. Distribution and behaviour of glabrous cutaneous receptors in the human foot sole. *The Journal of Physiology*, 583(3), 2002.

[17] T. A. Kern. Modeling the User. *Engineering Haptic Devices (T. A. Kern, Ed.), Springer-Verlag*, 2009.

[18] K. Kuchenbecker, J. Fiene, and G. Niemeyer. Improving contact realism through event-based haptic feedback. *IEEE Transactions on Visualization and Computer Graphics*, 12(2):219–230, 2006.

[19] M. Magana and R. Velazquez. On-shoe tactile display. In *IEEE Intl Workshop on Haptic Audiovisual Environments and Games*, 2008.

[20] M. Mahvash and V. Hayward. Haptic rendering of cutting: A fracture mechanics approach. *Haptics-e*, 2(3):1–12, 2001.

[21] D. Marigold and A. Patla. Adapting locomotion to different surface compliances: neuromuscular responses and changes in movement dynamics. *Journal of neurophysiology*, 94(3):1733, 2005.

[22] L. Meirovitch. *Dynamics and control of structures*. John Wiley & Sons, 1990.

[23] A. Nashel and S. Razzaque. Tactile virtual buttons for mobile devices. In *Proceedings of CHI*, pages 854–855. ACM, 2003.

[24] I. Poupyrev, S. Maruyama, and J. Rekimoto. Ambient touch: designing tactile interfaces for handheld devices. In *Proceedings of UIST*. ACM, 2002.

[25] A. Priplata, J. Niemi, J. Harry, L. Lipsitz, and J. Collins. Vibrating insoles and balance control in elderly people. *The Lancet*, 362(9390):1123–1124, 2003.

[26] S. Rapoport, J. Mizrahi, E. Kimmel, O. Verbitsky, and E. Isakov. Constant and Variable Stiffness and Damping of the Leg Joints in Human Hopping. *Journal of Biomechanical Engineering*, 125, 2001.

[27] A. Rovers and H. Van Essen. Guidelines for haptic interpersonal communication applications: an exploration of foot interaction styles. *Virtual Reality*, 9(2):177–191, 2006.

[28] J. Sabatier and A. Ekimov. A Review of Human Signatures in Urban Environments Using Seismic and Acoustic Methods. In *2008 IEEE Conference on Technologies for Homeland Security*, pages 215–220, 2008.

[29] V. Stiles, I. James, S. Dixon, and I. Guisasola. Natural Turf Surfaces: The Case for Continued Research. *Sports Medicine*, 39(1):65, 2009.

[30] U. Stobener and L. Gaul. Modal vibration control for PVDF coated plates. *Journal of Intelligent Material Systems and Structures*, 11(4):283, 2000.

[31] N. Tanaka and T. Sanada. Modal control of a rectangular plate using smart sensors and smart actuators. *Smart Materials and Structures*, 16(1):36–46, 2007.

[32] J. Taylor and Q. Huang. *CRC handbook of electrical filters*. CRC, 1997.

[33] H. Tramberend, F. Hasenbrink, G. Eckel, U. Lechner, and M. Goebel. CyberStage – An Advanced Virtual Environment. *ERCIM News*, 31, October 1997.

[34] M. Trulsson. Microreceptive afferents in the human sural nerve. *Exp Brain Res*, 137:111–116, 2001.

[35] Y. Visell. Tactile sensory substitution: Models for enaction in HCI. *Interacting with Computers*, In press, 2008.

[36] Y. Visell, J. Cooperstock, B. Giordano, K. Franinovic, A. Law, S. McAdams, K. Jathal, and F. Fontana. A Vibrotactile Device for Display of Virtual Ground Materials in Walking. In *Proceedings of Eurohaptics*, 2008.

[37] Y. Visell, F. Fontana, B. Giordano, R. Nordahl, S. Serafin, and R. Bresin. Sound design and perception in walking interactions. *International Journal of Human-Computer Studies*, 2009.

[38] Y. Visell, A. Law, and J. Cooperstock. Touch Is Everywhere: Floor Surfaces as Ambient Haptic Interfaces. *IEEE Transactions on Haptics*, 2009.

[39] Y. Visell, A. Law, J. Ip, S. Smith, and J. R. Cooperstock. Interaction Capture in Immersive Virtual Environments via an Intelligent Floor Surface. In *Proc. of IEEE Virtual Reality*, 2010 (To appear).

[40] Y. Visell, S. Smith, A. Law, R. Rajalingham, and J. R. Cooperstock. Contact Sensing and Interaction Techniques for a Distributed, Multimodal Floor Display. In *Proc. of IEEE 3D User Interfaces*, 2010 (To appear).

[41] H. Yao, V. Hayward, and R. Ellis. A tactile enhancement instrument for minimally invasive surgery. *Computer Aided Surgery*, 10(4):233–239, 2005.